Nanoscale Advances

Accepted Manuscript

This article can be cited before page numbers have been issued, to do this please use: R. Davarnejad, K. Haghighatnejad, O. Sartipzadeh Hematabad, Z. Mohammadpour, M. Komijani and J. Kennedy, *Nanoscale Adv.*, 2026, DOI: 10.1039/D5NA00776C.

ROYAL SOCIETY OF CHEMISTRY

rsc.li/nanoscale-advances

View Article Online
DOI: 10.1039/D5NA00776C

Synthesis of Pluronic F127 Copolymer/Iron Oxide-GelMA Nanocomposite for Doxorubicin Drug Delivery

Reza Davarnejad*[1, 2], Kimia Haghighatnejad[2], Omid Sartipzadeh Hematabad[1, 3], Zahra Mohammadpour**[4], Majid Komijani[2, 5], John F. Kennedy[6]

[1]Department of Chemical Engineering, Faculty of Engineering, Arak University, Arak 38156-8-8349, Iran
[2]Nanobiotechnology Group, Multi-disciplinary and Interdisciplinary Department, Arak University, Arak 38156-8-8349, Iran
[3]Biomaterials and Tissue Engineering Research Group, Department of Interdisciplinary Technologies, Breast Cancer Research Center, Motamed Cancer Institute, ACECR, Tehran 15179-64311, Iran
[4]Medical Nanotechnology Department, Breast Cancer Research Center, Motamed Cancer Institute, ACECR, Tehran, 1517964311, Iran
[5]Department of Biology, Faculty of Science, Arak University, Arak, 38156-8-8349, Iran
[6]Chembiotech Laboratories, Kyrewood House, Tenbury Wells, WR15 8SG Worcester, UK

Abstract

In this research a drug polymeric nanocarriers system consisting of Pluronic F127 copolymer /GelMA iron oxide nanoparticles was prepared to load and release doxorubicin. Various weight ratios of the polymer were used to find the highest drug entrapment rate and an optimal size of composite. The results showed that the maximum rate of drug entrapment in the system was at 57 %. Furthermore, GelMA was synthesized and analyzed by FTIR and FESEM. Various weight ratios of gel were used to obtain an optimal concentration, as well. The swelling rate and degradability of hydrogels were considered. It was found that GelMA with concentration of 10% had more swelling and degradability. Therefore, it was chosen as the optimal concentration. Finally, the drug system was considered by FTIR, FESEM, XRD, TGA and VSM. The results showed that the drug system had slow release and this followed the Korsmeyer-Peppas mechanism.

Keywords: Pluronic, GelMA, Controlled release

*Corresponding authors:
Email: *r-davarnejad@araku.ac.ir, rdavarne@uwo.ca, reza_davarnejad@yahoo.com.ph

**mohammadpour@acecr.ac.ir
Tel.: +98-9188621773
Fax: + 98-86-34173450

View Article Online
DOI: 10.1039/D5NA00776C

1. Introduction

Various methods have been used to treat cancer disease such as surgery, radiotherapy and chemotherapy[1]. However, chemotherapy as one of the most important methods is usually applied but, its success depends on the drug delivery system and the type of cancerous tumor[2,3]. The favorable characteristics of drug delivery systems such as natural access, controlled release and low toxic effects increased their applications[4]. An ideal drug delivery system should load the drug and exactly transfer it to the target organ. The drug nanocarriers significantly lead to the continuous and controlled drug release with maintaining the drug level. They interact on the surface and inside the biological cells. They may deeply penetrate in a tissue due to their small size[5].

Alexandridis et al. found that the micelle formation thermodynamically is as a positive entropy process[6]. Linse discussed the critical micelle concentration (CMC), critical micelle formation temperature (CMT), number of aggregation and different hydrodynamic radius of the Pluronic block copolymers in aqueous solutions[7]. Shen et al. investigated controlled release of doxorubicin (DOX) loaded on Zein[8]. Sheikh et al. considered the drug entrapment, release, and retention efficiency in terms of transition metal ion content and morphology of doxorubicin in the liposomal system and its therapeutic potential[9].

Mosafer et al. conjugated doxorubicin-carrying PLGA-coated SPIONs to the AS1411 aptamer. They successfully tested it on the intestinal carcinoma cells of various categories of mice[10,11]. Alyane et al. prepared nanoliposomes containing doxorubicin using a gradient method[12]. They used the nanoliposomes with 100 nm size and could entrapment the drug around 90%. Haghiralsadat et al. loaded doxorubicin into liposomal carriers for affecting the bone cancer[13]. They produced nanosystems with size of 126 nm and encapsulation efficiency of 89%. The maximum release of doxorubicin was around 46% for 48 h. Saravanakumar et

View Article Online
DOI: 10.1039/D5NA00776C

al. successfully delivered doxorubicin to a cancer cell line using polylactic-glycolic acid nanoparticles attached to the AS1411 aptamer[14].

Pluronic F127 micelles, GelMA hydrogels and iron oxide nanoparticles have each been extensively investigated for drug delivery due to their unique properties such as thermoresponsiveness, biocompatibility and magnetic guidance although these systems showed some limitations in drug loading efficiency, controlled release and multifunctionality when they individually used[15].

Carrera Espinoza et al. successfully delivered doxorubicin to a cancer cell line using smart supermagnetic nanocomposites based on iron oxide nanoparticles coated with Pluronic F127[16]. They increased the drug release at acidic pHs. This may be due to the pH sensitivity of polymer. According to the in vitro results, a survival rate of 90% in HepG2 cells treated with the nanocomposite was observed. Furthermore, the synthesized smart nanocomposite showed a drug delivery to the liver cancer overcoming the limitations of traditional therapies.

In this research, a composite system combining Pluronic F127, GelMA and iron oxide nanoparticles, which leverages the synergistic advantages of each component was prepared and applied. The thermoresponsive Pluronic F127 provides enhanced drug entrapment and release control, GelMA hydrogels offer a tunable and biocompatible network, and iron oxide nanoparticles introduce magnetic responsiveness for good potential guided delivery[17].

According to the literature on the doxorubicin carriers such as liposomes or polymeric nanoparticles, it seems that the hybrid system proposed in this research can show better characteristics such as higher drug loading efficiency, tunable particle size and pH-responsive release[15]. Likewise, a system based on Pluronic F127 copolymer/iron oxide-Gelatin Methacrylate (GelMA) nanocomposite for the drug delivery was made. Various analyses such as FTIR, FESEM, XRD, TGA and VSM were used to investigate the physico-chemical

View Article Online
DOI: 10.1039/D5NA00776C

properties of the doxorubicin medicinal system. Then, the kinetics of doxorubicin release through it was investigated in an aqueous environment.

Therefore, the aim of this study is to develop an optimized Pluronic F127 / GelMA / iron oxide nanoparticle nanocarrier with enhanced drug encapsulation, controlled release behavior and good potential for the improved therapeutic performance.

2. Materials and methods

Doxorubicin-HCl (DOX) [$C_{27}H_{29}NO_{11}\cdot HCl$, 98%-102%, (50 mg/25 ml)] was purchased from EBEWE Pharma Co. Pluronic® F-127 (PF) [$(C_3H_6O\cdot C_2H_4O)_x$, Bio-Reagent], Sodium Acetate (CH_3COONa, ≥ 99.0%), Ethylene Glycol ($C_2H_6O_2$, ≥ 99.0%), and Ferric chloride hexahydrate ($FeCl_3\cdot 6H_2O$, 98%) were used as the precursors and precipitating agent of magnetic nanoparticles coated, Gelatin (Bovine Skin, Type B), Methacrylic Anhydride (MA) ($C_8H_{10}O_3$, ≥ 98.0%), Ethylenediaminetetraacetic acid (EDTA) ($C_{10}H_{16}N_2O_8$, ≥ 98.0%), Sodium bicarbonate ($NaHCO_3$, 99.5%), and phosphate-buffered saline (PBS, pH=7.4) were applied as GelMA synthesis, as well. 2-Hydroxy-4′-(2-hydroxyethoxy)-2-methylpropiophenone (Irgacure2959, 98.0%), Diphenyl(2,4,6-trimethylbenzoyl) phosphine oxide (TPO, 97.0%), Methanol (MetOH, 99.0%), and Ethanol (EtOH, 96.0%) were utilized as the photoinitiator, dissolving and washing agent, respectively.

2.1. Synthesis of GelMA

A tablet of PBS was dissolved in 500 ml of deionized (DI) water to set the pH on 7.4. Then, 100 ml of the above solution mixed with 10 g of gelatin powder and stirred with a magnetic stirrer with 400 rpm at a temperature of 60 °C for 2 h. Then, 10 ml of MA was dropwise added to the solution with a syringe pump. The solution temperature was reduced to 55 °C and stirred for 3 h, as well. The solution was diluted with DI with a ratio of 1/4 (v/v) to stop the reaction and continuously stirred for 1 h. The synthesized Gelatin Methacryloyl (GelMA)

View Article Online
DOI: 10.1039/D5NA00776C

was added into the dialysis tubing. For dialysis bag preparation, 0.84 g of Sodium bicarbonate and 0.372 g of EDTA were dissolved in 200 ml of DI water and stirred to obtain a clear and uniform solution. The solution was heated on a stirrer-heater to boil. The dialysis bag was added to the boiling solution. The dialysis bag was boiled for 30 min and finally washed with DI water to remove the excess material[18]. The solution of synthesized GelMA was added into the dialysis bag and kept in the oven at 45 °C for one week. The safe handling, storage and disposal of methacrylate anhydride have been shown in Fig. S1 (Supplementary Materials Section).

Dialysis bag (with cut-off 14 kDa) was performed to remove possible residual toxic impurities such as methacrylate anhydride, by-products and unreacted monomers. Since all undesirable substances in the dialysis bag except GelMA have a molecular size smaller than the size of the dialysis bag, they will be permeated out of the bag due to the concentration difference (inside and outside the bag) when the bag is placed in the DI water. Furthermore, the water in the dialysis chamber is replaced every 6 h to increase the GelMA purification from undesirable substances. The material was emptied from the dialysis bag after 7 days and freeze-dried to find a uniform powder of GelMA.

2.2. Swelling index of GelMA

Three different concentrations of GelMA, 10, 15, and 20% (w/v), were prepared by adding GelMA powder to 5 ml PBS (pH=7.4) and stirring for 15 min at 45 ˚C until a homogeneous solution was obtained[19]. Then, 20 mg of photo-initiator TPO was dissolved in 0.5 ml of MeOH and placed on the stirrer, and then 20 mg of photo-initiator Irgacure was added to the TPO solution to obtain a uniform solution. Afterwards, the photo-initiator solution by 0.1% w/w was added to each of the GelMA solutions with different concentrations. Finally, the solution was irradiated under the UV light (250 W, NOOR, Iran) at a rectangular cube mould made of PTFE with dimensions of 12×12×4 mm for 20 min to create gel.

View Article Online
DOI: 10.1039/D5NA00776C

The samples obtained from the previous stage were initially weighed and then immersed in 15 ml of PBS solution (pH = 7.4). The lid of the beakers was tightened with aluminum foil and placed in an incubator at 37 °C for 48 h. The samples were taken out and poured on the filter paper to remove water from them, and then weighed. Moreover, they were placed in a 37 °C incubator for 10 min to evaporate the surface liquid on the GelMA and weighed again. The swelling of the gel will be determined by:

$$Swelling\ Capacity\ \% = \frac{W_t - W_d}{W_d} \times 100 \quad (1)$$

where, w_t and w_d are the weights of hydrated samples versus time and the initial dry one, respectively.

2.3. Degradation index of GelMA

Various concentrations of GelMA are firstly poured and cured in the mould. Then, they are weighed and placed into 10 ml of PBS solution. According to the static incubation, the containers are tightly sealed with aluminum foil and placed in an incubator at 37 °C. The sampling process follows as on the first day, 200 µl of the solution from each container is removed and transferred to 0.5 ml microtubes and then replaced with 200 µl of fresh PBS solution. This process is repeated daily for 90 days. Finally, the contents of the containers are centrifuged at 4000 rpm for 10 min at room temperature (25±1 °C). The supernatant is discarded, and the residue is washed three times with DI water. The remaining solid is dried in an oven at 37 °C overnight, weighed, and the degradation percentage of each sample is calculated using the following relation:

$$Biodegradation\ \% = \frac{W_d - W_t}{W_d} \times 100 \quad (2)$$

where, w_d and w_t are the weights of the initial dry and time one, respectively.

View Article Online
DOI: 10.1039/D5NA00776C

2.4. Synthesis of PF-coated magnetic nanoparticles (MNPs)

1.23 g of $FeCl_3.6H_2O$ was poured into a two-mouthed flask. Then, 75 ml of ethylene glycol was added to the flask and stirred to obtain a uniform solution under neutral gas (N_2). Then, 3.66 g of dry sodium acetate was added to the solution and stirred vigorously with a mechanical stirrer for 1 h. Subsequently, the yellowish solution was heated in a Teflon-lined stainless-steel autoclave at 200 ℃ for 16 h. The solution was removed from the autoclave and poured into a beaker, and washed several times with DI water and EtOH. The final products were dried in a vacuum oven for overnight at 37 °C. PF was dispersed by sonication process in DI water for 30 min to produce a uniform solution with various concentrations, 1%, 2% and 5% w/w. The surface-modified MNPs with PF were formulated using three different concentrations of polymer, mixed with 100 mg of MNPs, and stirred overnight. The MNPs coated with PF were washed numerous times with EtOH and DI water. Finally, the nanocomposites (MNPs-PF-1, MNPs-PF-2, and MNPs-PF-5) were dried at 65 ℃ overnight[16].

2.5. Preparation of DOX-loaded MNPs-PF

6 mg of each sample (MNPs-PF-1, MNPs-PF-2, and MNPs-PF-5) was separately mixed with 1 mg of DOX dissolved in 1 ml of water for injection. The solution had a natural pH of approximately 5.5 (within the range of 5.0–7.0), and no additional pH adjustment was performed to maintain DOX stability. The mixture was kept under constant shaking in a dark environment at room temperature for 48 h. The suspension was centrifuged at 2500 rpm for 5 min, and the supernatant solution was removed at the end of the loading period. The precipitate (DOX-loaded nanoparticles) was obtained by centrifugation at 13000 rpm for 10 min, and the acquired pellet was placed in an oven at 65 °C until its weight changes stabilized[16-1]. The drug concentration in the supernatant solution (floating on the surface) was measured using a UV-Vis spectrophotometer (Perkin Elmer America, Lambda 25) at

View Article Online
DOI: 10.1039/D5NA00776C

maximum absorption wavelength of 481 nm. The calibration curve of doxorubicin absorption versus its concentration was found. The drug-loading efficiency (DLE) and entrapment efficiency (EE) of DOX-loaded in the composites (nanoparticles) will respectively be calculated by:

$$Drug\ loading\ (\%) = \frac{weight\ of\ the\ loaded\ drug}{weight\ of\ the\ nanoparticles} \times 100 \quad (3)$$

$$Entrapment\ efficiency(\%) = \frac{weight\ of\ the\ loaded\ drug}{weight\ of\ the\ feeding\ drugs} \times 100 \quad (4)$$

2.6. Preparation of DOX-loaded MNP-PF/GelMA composite

DOX-loaded MNPs-PF/GelMA nanocomposites were prepared at three distinct weight percentages involving 10%, 15%, and 20% GelMA. 0.2 g of GelMA powder was added to 2 ml DI water and stirred till a homogeneous solution was obtained. Then, 0.1% (w/w) of the photoinitiator solution [(relative to GelMA) prepared in Section 2.2] was added to the solution and stirred for 10 min in the dark.

5 mg of DOX-loaded MNPs-PF (as prepared in Section 2.5) of each percentage of PF was added to GelMA with cross-linker agent and stirred vigorously for 30 min in a dark environment. Finally, the entire mixture was added to the PTFE mould and placed under a UV lamp at a distance of 10 cm for 20 min for the crosslinking step. GelMA was polymerized under UV light (250 W, UVA 360-405 nm) to form GelMA hydrogel.

2.7. Assessment of drug release in vitro

The determination of DOX release from MNPs coated with PF was conducted using the following method.

View Article Online
DOI: 10.1039/D5NA00776C

6 mg of desiccated DOX-loaded MNPs-PF were transferred to a 5 ml tube, and 2 ml of PBS solution was added to the tube. Subsequently, the tube was positioned on a roller stirrer at 37 °C. The samples were extracted from the solution at various time intervals to quantify the DOX release in the solution. Following each sample, an equivalent volume of new buffer was added to ensure the medium's concentration remained constant. The released drug (DOX) content was quantified by detecting its absorbance at 485 nm using the UV-Vis spectrometer. Calibration curves were generated for the medications using standard methods under controlled experimental circumstances. The medication release (%) is calculated as:

$$Cumulative\ drug\ release\ \% = \frac{weight\ of\ drug\ release\ (mg)}{weight\ of\ total\ drug\ (mg)} \quad (5)$$

2.8. Release mechanism

The mathematical modeling should be a very useful issue because it allows predicting the release kinetics. In fact, it would be possible to measure some important parameters such as the drug diffusion coefficient. Therefore, mathematical modeling requires a sufficient understanding of all phenomena affecting the drug release kinetics. The kinetics of drug release from the carriers depends on some factors such as the geometric structure of matrix, type of drug and drug release mechanism. There are several kinetic release models such as zero-order[20], first-order[21,22], Higuchi[23] and Korsmeyer-Peppas[24] for drugs. Several renowned mathematical models were evaluated to investigate the mechanism of DOX release from composites, as detailed below:

- **Zero-order model**

The model explains samples that release rate of the drug is autonomous of the dosage of the soluble medicine. This model is shown as:

View Article Online
DOI: 10.1039/D5NA00776C

$$Q_t = K_0 t \quad (6)$$

where, t and K_0 are time and the rate constant of zero-order model, respectively. Q_t is the cumulative value from the drug released at time of t.

- **First-order model**

The model explains samples that rate of release depends on drugs like DOX. This pattern is shown as:

$$\log(Q_t) = -\frac{K_1 t}{2.303} \quad (7)$$

where, K_1 and t are the first-order velocity constant and time, respectively. Q_t is the cumulative value from the drug remaining at time of t.

- **Higuchi model**

The release of a drug depends on the time. In this case, the drug release mechanism depends on Fick's law. The model is shown using:

$$Q_t = K_H t^{0.5} \quad (8)$$

where, K_H represents the initial constant speed, and t denotes time. Q_t refers to the accumulated amount of the drug discharged at a specific time of t.

- **Korsmeyer-Peppas release model**

The Korsmeyer-Peppas model is utilized to gain a better insight from release mechanism of the drug. According to the power law model, this elucidates how drugs are released from polymeric systems. This model is particularly useful for characterizing systems with multiple mechanisms or unclear release processes. This model is illustrated as:

View Article Online
DOI: 10.1039/D5NA00776C

$$Q_t = K_{KP}.t^n \quad (9)$$

where, K_{KP}, t, and n are the rate constant of Korsmeyer-Peppas, time, and the release exponent. Q_t is the cumulative amount of drug released at time of t.

2.9. Characterization

Fourier Transform Infrared spectroscopy (FTIR) is used to analyze the functional groups and their role in the adsorption process. The Scanning Electron Microscope (SEM) will be applied to examine the nanocomposite surface characteristics and morphology. Magnetic behavior of iron oxide nanoparticles and combination of nanoparticles and polymer may be studied by the Vibrating Sample Magnetometer (VSM). X-ray Diffraction (XRD) technique will be used to identify the crystal structure. Thermogravimetric analysis (TGA) of iron oxide under argon atmosphere with heating rate of 10 °C /min is also done in the temperature range of 25-600 °C.

2.10. Cell cytotoxicity study

The human breast cancer MCF-7 cell line [provided by the Pasteur Institute of Iran (Tehran)] was grown in DMEM High Glucose medium (Gibco) supplemented with 10% fetal bovine serum (FBS) (Gibco) and penicillin/streptomycin 1% (Gibco) in a humidified incubator under temperature of 37 °C, relative humidity of 90%, and CO_2 5%. The cells were prepared by washing in PBS when they reached confluence, and they were separated from the dish using trypsin-EDTA (Gibco). The cells were then resuspended to achieve a concentration of 1×10^4 cells/ml after being moved to a centrifuge tube and spun for 5 min at 1100 rpm. MCF-7 cells were seeded in a 96-well plate at a density of 1×10^3 cells per well, 24 h before the in vitro cytotoxicity studies. MNPs formulation coated with PF with 1%, 2%, and 5% concentrations loaded with the DOX prepared with PBS (pH 7.4 and 5.5) as described above. Control formulations without the DOX were also prepared using the same procedure. The four stock

View Article Online
DOI: 10.1039/D5NA00776C

solutions were filtered through sterile 0.22 µm Millipore paper, and then further diluted with sterile PBS (pH 7.4 and 5.5) step wisely to make the DOX concentrations in the range of 3.125-200 mg/ml. 100 µl of the DOX formulations and 100 µl of the culture medium (DMEM Medium + 10% FBS) were added to the cells to evaluate their cytotoxic effects. As the control, 100 µl of PBS (pH 7.4 and 5.5) was added to the cells as well as 100 µl of the culture medium. The cells were incubated for 24, 48, and 72 h at 37 °C in a humidified atmosphere with CO_2 5%. After incubation, the number of viable cells was determined by 3-(4,5-Dimethylthiazol-2-yl)-2,5-diphenyltetrazolium bromide (MTT) colorimetric assay.

20 µl of MTT solution (5 mg/ml) was added to each well. The plates were incubated for an additional 4 h, and then the medium was discarded. A volume of 150 µl of DMSO (dimethyl sulfoxide) was added to each well, and the solution was vigorously mixed to dissolve the reacted dye. The absorbance of each well was read on a microplate reader (BioTek Instruments, ELx800, USA) at a test wavelength of 570 nm and reference wavelength of 650 nm. The samples were tested in triplicate, and six wells with only culture medium served as blanks. The relative cell viability (%) is calculated as:

$$Cell\ Viability\ (\%) = \frac{A_{of\ treated\ cells}}{A_{of\ untreated\ cells}} \times 100 \quad (10)$$

2.11. Statistical analyses

Analysis of variance (Two-way ANOVA) was applied for statistical analysis. Data were analyzedin triplicate and are presented as mean ± standard deviation (SD). The data obtained at $p \leq 0.05$ were considered statistically significant.

3. Results and discussion

3.1. Characterization of MNPs and DOX-MNPs-PF/GelMA composite

View Article Online
DOI: 10.1039/D5NA00776C

In order to study the nature of obtained product, XRD analysis was performed on MNPs. As shown in Fig. 1a, the specific peaks of Fe_3O_4 at 2θ are 30.24°, 35.52°, 43.12°, 53.48°, 57.16° and 32.68° which are corresponding to the Miller indices of the reflection plane of (220), (311), (400), (422), (511), (440), respectively.

The Fe_3O_4 magnetic nanoparticles form a cubic crystal structure[18,25]. The magnetic properties of MNPs and the MNPs coated with various percentages of PF (1%, 2%, and 5%) were investigated by the VSM technique. As shown in Fig. 1b, the magnetic values of pure MNPs and the composite of MNPs-PF nanoparticles were at 50.98, 42.59, 36.71, and 25.76 emu/g, respectively. The decrease in the magnetic value in the composite is due to the polymer coating. The magnetic property of the nanocomposite should be sufficient because a rapid separation was observed by applying an external magnetic field.

One of the techniques for identifying the structure of magnetic nanoparticles is TGA. This measures changes in the weight of sample with temperature. Fig. 1c shows the thermal calorimetry technique for Fe_3O_4 nanoparticles. As shown in this figure, weight loss less than 300 °C probably is related to the hydroxyl groups evaporation and separation of adsorbed solvents[6].

According to Fig. 1d, PF has two individual peaks. A peak at 2885 which belongs to C-H stretching vibrations and a peak at 1250 cm^{-1} which belongs to C-O stretching vibrations[16]. There are some peaks at 580, 3400 and 1630 cm^{-1} due to iron oxide presence in the mixture while the peaks at 1250 and 2885 cm^{-1} are due to PF presence in the composite. Moreover, the intensity of the peaks of 5% PF concentration is much higher than that of 1% and 2%PF in the composite[16].

DLS analyses were performed for nanocomposites of pure MNPs and MNPs coated with DOX-loaded PF (three different concentrations). The polydispersity index (PDI) and average

View Article Online
DOI: 10.1039/D5NA00776C

diameter of the MNPs were at 189.3 nm and 0.217, respectively (Fig. 2a). After coating with PF, the PDI and average diameter for PF 1% were at 264.8 nm and 0.192 while for PF 2%, they were at 445.3 nm and 0.440, and for PF 5% were at 338.9 nm and 0.176, respectively (as shown in Figs. 2b-d), confirming the polymeric coating on the surface of the MNPs.

As the PF concentration increased, the average diameter also increased, indicating an effective coating on the surface of the nanocomposites, except for PF 5%, where the particle size decreased. This may be due to PF concentration increment and its amphiphilic nature. As the PF concentration increases, the number of hydrophilic groups of the PF chain that have the connectivity to bind to the surface of the MNPs increases. On the other hand, the hydrophobic functional groups in the PF chain come closer to each other, creating an interaction and repulsion, preventing further increase in binding between the PF and the MNPs. In fact, the hydraulic diameter is lower in the PF 5% coating than in the 2% coating. Furthermore, the effects of PF concentration (1, 2, and 5 w%) and pH (7.4 and 5.5) on zeta potential and particle diameter were shown in Table 1. The results indicated that an increase in PF concentration led to an increase in the average diameter and a diminution in zeta potential, except for PF 5%. This phenomenon can be attributed to the amphiphilic nature of the PF coating on the surface of the MNPs. Moreover, the covering polymer protected the surface charge of the MNPs, which led to a reduction in zeta potential. The zeta potential was increased and the average diameter of the particles was decreased when the pH was reduced to 5.5. Conversely, the pH increased to 7.4 (due to reducing the zeta potential) would increase the particle size. As a result, the produced nanocarrier has a high potential for delivering the DOX to acidic malignant human body tissues and is pH sensitive.

Fig. 3a shows FTIR analysis of gelatin. According to this, there is a peak at 3433 cm^{-1} which belongs to the hydrogen bond of water. The peaks in 3287 to 3292 cm^{-1} and in 1538 to 1633 cm^{-1} may be associated with amide, while the peaks in 1380 to 1460 cm^{-1} are attributed to

View Article Online
DOI: 10.1039/D5NA00776C

symmetric and asymmetric vibrations of the methyl group. In fact, gelatin is a type of proteins. They have amino acids which are connected by amide bonds. Amide bands represent different vibrational modes of peptide bonds. GelMA's absorption band is located in the amide group region as shown in Fig. 3a. A peak at 1243 cm^{-1} belongs to amide which is related to the vibration of the N-H bond. This partly is related to the N-C bond. A peak at 1555 cm^{-1} also belongs to amide. This is related to the N-H bonds, as well. A peak at 1645 cm^{-1} is also known as amide. It shows the vibration of the C=O bonds. The anhydride C=O bands observed in the crude sample peaks at 1812 and 1760 cm^{-1}, disappeared after dialysis, and no peaks corresponding to unreacted monomer/by-products were detected.

A peak at 3433 cm^{-1} represents O-H and N-H stretching vibrations. The peaks in 2800 to 3100 cm^{-1} belong to H (C-H) stretching vibration[26]. Furthermore, the peaks of 15% GelMA concentration are much more intense than those of 10% and 20% GelMA concentrations.

The FTIR spectrum of pure DOX has many distinctive peaks. O-H stretching vibrations occur at 3445 cm^{-1}, C-H stretching vibrations at 2918 cm^{-1}, and C=O bond vibrations at 1730 cm^{-1}. Aromatic C-H bending vibrations occur at 1420 cm^{-1}, C=C ring vibrations at 1627 cm^{-1}, C-O-C bond vibrations at 1077 cm^{-1}, and out-of-plane bending vibrations of C-H bonds in the anthracycline chromophore ring are noted at 814 cm^{-1}, as shown in Fig. 3b.

The presence of DOX and PF 2%-MNPs combination in the DOX-PF 2%-MNPs spectrum is also evident. The sharp peaks were observed in the regions of 2885 cm^{-1}, and 580 cm^{-1} which is related to aliphatic CH, showing MNPs. The peak of 3422 cm^{-1} is characteristic of the OH group, and the peak of 1638 cm^{-1} is associated with the C=O factor group. In the functional group of DOX, a wide peak was observed in the regions of 3436 cm^{-1}, and the peak of 1631 cm^{-1} represents the C=O factor group. Finally, in the DOX-PF 2%-MNPs/GelMA spectrum, a peak was observed in the regions of 3400 cm^{-1}, which indicates the presence of DOX, and a sharp peak around 2900 cm^{-1} proves the presence of NPs in the composite. In the blended

View Article Online
DOI: 10.1039/D5NA00776C

composite spectrum, the peaks of PF and GelMA, which are related to NH_2 and OH tensile vibrations, change to higher frequencies, which can lead to hydrogen bonds between the NH_2/OH group of PF, the NH_2/OH group of DOX, and or the OH group of GelMA.

Field Emission Scanning Electron Microscopy (FESEM) was used to examine the surface morphology, size and uniformity of samples. Fig. 4 shows that the composites have spherical morphology. The nanoparticles are aggregated due to their magnetic properties. The nanocomposites (with Pluronic) would be aggregated less than the pure nanoparticles. Its reason may be due to having a larger size of particles in the nanocomposite[16,18]. According to Figs. 4a-d, the average size of the MNPs and the nanocomposite will increase with increasing polymer concentration. This indicates the coating influence on the surface of nanocomposites. The mean diameter size of the MNPs was approximately at 208 nm (Fig. 4a), while it respectively increased to 282, 404 and 315 nm in coated ones with PF of 1%, 2%, and 5%. According to Figs. 4e & 4f, PF 2%-MNPs-DOX were completely and uniformly dispersed in the GelMA composite.

3.2. GelMA swelling

The swelling test of GelMA hydrogel was investigated by 48 h. The swelling rate of hydrogels is one of the important aspects of their medical applications because changes in it will affect their surface properties and mobility. Moreover, it affects the solvent ability to penetrate into the hydrogels. The swelling rate in hydrogels is a function of polymer porosity and the interaction of solvent and polymer[27]. Swelling data of several samples with 10%, 15% and 20% GelMA were illustrated in Table 2 (and Table S1). All samples were exposed to ultraviolet light under identical conditions as 365 nm, irradiation time of 20 min, and room temperature.

View Article Online
DOI: 10.1039/D5NA00776C

The swelling rate sharply decreased with increasing the initial concentration of GelMA. In fact, higher GelMA concentrations produce hydrogels with greater density and a higher degree of crosslinking. Moreover, photoinitiator weight ratio increment would be led to more dangling functional groups of the polymer per unit volume of it during the curing process. This would increase the swelling, compaction, and crosslinking. Furthermore, the pore size of hydrogel would decrease, as well[28].

The swelling behavior of the GelMA-based nanocomposite plays a critical role in controlling the drug-release mechanism. As the hydrogel absorbs water and exhibits a higher swelling ratio, the increased water uptake promotes polymer-network relaxation and enlarges the mesh size of the matrix. This structural loosening facilitates the diffusion of DOX molecules through the hydrogel and results in an accelerated release profile. Therefore, the swelling characteristics are directly correlated with the degradation-mediated drug-release behavior of the composite, and understanding this relationship is essential for predicting the therapeutic performance of the system.

3.3. GelMA degradation

Degradation data of various samples with 10, 15 and 20% GelMA were illustrated in Table 3 (and Fig. S2 & Table S2). The amount of photoinitiator and the duration of exposure to ultraviolet light were also considered under the constant conditions. The degradation of GelMA hydrogels was monitored at various concentrations over a period of 90 days to evaluate the long-term stability and degradation behavior of the hydrogels. The results showed that the degradation rate would sharply decrease with increasing the initial concentration of GelMA. The destruction rate may be supported with a similar analysis as mentioned for the swelling behavior.

View Article Online
DOI: 10.1039/D5NA00776C

The hydrogel's equilibrium water content dropped in proportion to the GelMA concentration. The interconnecting GelMA network chains in the hydrogel were densely packed to create a denser network structure as the GelMA concentration rose. The hydrogel's equilibrium water content fell as a result of the hydrogel's lower porosity, which also lessened the swelling effect of water molecules on the hydrogel to some degree.

After the degradation of the GelMA hydrogel, the DOX-loaded MNP-PF nanoparticles are gradually released into the surrounding environment. Depending on their size, surface functionality, and concentration, these nanoparticles can undergo different biological fates. They may be internalized by cells and processed through lysosomal pathways, or they can be cleared through the reticuloendothelial system (primarily the liver and spleen). Although MNP-based systems are generally considered biocompatible, potential concerns such as local particle accumulation, oxidative stress, or inflammation at high doses should be taken into account. These considerations are important for the long-term biosafety of MNP-based drug-delivery platforms.

3.4. Drug entrapping

Fig. 5 shows UV-Vis spectrometer spectra to determine a successful encapsulation of DOX. As shown in Fig. 5a, the calibration curve of the free DOX based on the serial dilution method has been plotted as a function of its absorption intensity at a wavelength of 485 nm. The PF-MNPs and three samples of each percentage of PF in PF-MNPs-DOX nanocomposites were compared to free DOX, as shown in Figs. 5b-d. The results revealed a DOX-related absorbance peak at 485 nm associated with the PF 1%-MNPs-DOX, PF 2%-MNPs-DOX, and PF 5%-MNPs-DOX, confirming a successful DOX encapsulation.

Regarding the remaining drug, it should be noted that DOX release occurs in two stages. The first stage involves an initial burst release due to swelling and diffusion from the hydrogel

View Article Online
DOI: 10.1039/D5NA00776C

matrix. The second stage corresponds to the sustained release of the remaining drug which is closely associated with the progressive degradation of the hydrogel over the 90-day period. Therefore, the remaining drug is gradually released as the hydrogel network breaks down, providing a controlled and extended drug release profile.

As illustrated in Table 4, the entrapment efficiency (EE) and drug loading efficiency (DLE) were maximally found at 74.73±0.549 and 2.60±0.019 [Table S3 (average of 3 repetitions)] for PF 2% composite with iron oxide nanoparticles, respectively. The drug loading process was mainly based on the physical adsorption mechanism inside the nanoparticles[29]. In the controlled release of drug, the patient does not suddenly receive a high dose of drug after taking it. In fact, the drug would be released to a suitable dose and this remains constant over time. According to the in vitro study, the highest release rate of DOX from the nanocomposite (with PF 2%) was around 74.73±0.549 after 48 h at pH of 7.4 and 37 °C.

3.5. In vitro evaluation of drug release

Three samples of nanoparticles with different concentrations of PF were prepared to investigate the release of DOX from the nanoparticles. The effect of various percentages of PF used in the nanoparticles on the amount of drug release was investigated. The release behavior of DOX from the nanoparticles was evaluated at a pH of 7.4. The variation in release demonstrated that the DOX-loaded PF-MNPs composite functioned as a PF concentration-responsive delivery system influenced by ingredient concentration. Fig. 6a shows the DOX release profile from nanoparticles at three different ratios of PF. The DOX release grew up with increasing PF percentage. Consequently, the release of DOX was respectively enhanced to 47.63%, 52.74%, and 50.99% at 1%, 2%, and 5% of PF at pH of 7.4 over a period of four days. The minimal release of DOX at pH of 7.4, which corresponds to the pH of blood and normal tissues, contributed to reducing the adverse side effects

View Article Online
DOI: 10.1039/D5NA00776C

associated with DOX as a powerful anti-cancer agent. The cumulative DOX release of DOX-loaded MNPS blended with 1%, 2%, and 5% of PF had an analogous pattern before 10 h.

It is well established that the extracellular pH of cancerous tissue is lower than that of healthy tissue. Several researchers have attempted to create pH-responsive delivery carriers to take advantage of this disparity. The profile of DOX release at different pH conditions (7.4 and 5.5) was used just for PF 2%-MNPs-DOX due to its higher DLC percentage. Correspondingly, as illustrated in Fig. 6b, the in vitro release of DOX from the PF 2%-MNPs–DOX showed sustained release patterns under acidic (pH=5.5) and neutral (pH=7.4) conditions. The drug release for pH of 5.5 was much higher than that of pH of 7.4. After 24 h of release, more than 42% of the total drug was liberated in pH of 5.4. Furthermore, the DOX release from the PF 2%-MNPs was pH sensitive, showing a slower release rate in neutral conditions than in the acidic ones. These met recent findings regarding stronger hydrogen bonding contact at neutral pH and the higher solubility of DOX in the acidic environments[30,31].

3.6. Drug release modeling

In this research, the drug release mechanism was studied through the kinetic models (zero-order, first-order, Higuchi, Korsmeyer–Peppas). This examination involved fitting the experimental release data at a pH of 7.4 using Eqs. (6-9) associating with graphs of Fig. 7. The exponent value in the Korsmeyer-Peppas model shows that the release mechanismis governed by Fick's law (diffusion) when $n \leq 0.34$, while it follows case II transport, involving the swelling and relaxation of the polymer matrix when $n \geq 0.85$. It indicates an anomalous mechanism, combining Fickian diffusion with polymer matrix erosion when $0.34 < n < 0.85$.

View Article Online
DOI: 10.1039/D5NA00776C

The Korsmeyer-Peppas model was selected to describe the drug release from GelMA-based hydrogels due to its suitability for hydrophilic polymer systems where drug release occurs via a combination of diffusion and polymer swelling. This model has been widely validated in similar hydrogel-based drug delivery studies, providing insights into the release mechanism through the diffusional exponent n[32].

As shown in Table 5, the Korsmeier-Peppas model has the highest R^2 (≈1) compared with the other models for PF 2% nanocomposite (which had the maximum EE% and DLE%). Furthermore, its power value (n) was calculated as 0.7497, 0.7120, and 0.7418 for PF 1%, 2%, and 5%, respectively. This indicates that the release mechanism follows the anomalous mechanism[33]. In other words, the mechanism is based more on polymer matrix erosion than on Fickian transport.

The final data revealed better DOX release under acidic conditions, which can be attributed to the pH sensitivity of PF 2%. Additionally, the results confirmed the long-term release of DOX from the nanocomposites, which is crucial for reducing side effects and boosting drug accumulation in tumour tissues, and also demonstrated the controlled release capabilities of PF 2%-MNPs-DOX in acidic circumstances. For the stability consideration of drug loaded in the PF 2%-MNPs-DOX nanocarrier under acidic (pH=5.5) conditions, DOX-release data were measured by four different kinetic models involving zero-order, first-order, Higuchi, and Korsmeyer–Peppas models. They were evaluated with their results under neutral (pH=7.4) conditions as shown in Fig. 8.

As illustrated in Table 5, the power value (n) for PF 2%-MNPs under acidic (pH=5.5) conditions was at 0.5649 which indicates that the release mechanism follows combining Fickian diffusion with polymer matrix erosion. Compared to the calculated power under neutral (pH=7.4) conditions, which is more polymer erosion than Fickian diffusion, drug

View Article Online
DOI: 10.1039/D5NA00776C

release in an acidic environment follows both mechanisms. This results in more stable drug release.

3.7. Cell cytotoxicity

To evaluate the pharmacological activity and in vitro biocompatibility of the nanocarrier, an MTT assay was performed. The PF 2%-MNPs-DOX nanocarrier was chosen for this investigation due to its high DLC and EE (2.59 and 74.72%, respectively). The assay was carried out by increasing concentrations of DOX in the PF 2%-MNPs-DOX nanocarrier. As revealed in Fig. 9, the in vitro viability of MCF-7 cancer cells after 24, 48 and 72 h treatment with DOX formulated in MNPs PF 2%, and carrier without DOX.

As shown in Fig. 9a, few general outcomes was immediately made. The DOX carrier exhibited greater cytotoxicity at an acidic (pH=5.5) condition than at neutral (pH=7.4) one, especially at the highest concentration (200 μg/ml). The cellular viability of the DOX carrier was approximately 40% while it was more than 80% in the other pHs ($P<0.01$). The results illustrated significant time and concentration-dependent cell growth inhibition for the acidic (pH=5.5) environments. The similar trend of cytotoxicity can be observed for 48 and 72 h, as well. As shown in Fig. 9d, the data exhibited nontoxic effects after 24 h for both pHs. Consequently, it could be anticipated that in vivo PF-covered MNPs would be far less toxic than the other vehicles. if so, then the administration of DOX-loaded PF-MNPs nanocarriers at higher drug doses would be possible.

4. Conclusions

This research aimed to synthesize a suitable system for loading and releasing the doxorubicin as a cancer treatment medicine. For this purpose, a nanocomposite based on Pluronic F127 copolymer/iron oxide-GelMA nanoparticles was synthesized and characterized, successfully.

Several parameters, such as various polymer concentrations, pH and drug loading time, were investigated. Iron oxide nanoparticles were synthesized by the hydrothermal method and then composited with polymer by the ultrasonication process. Several tests confirmed nanocomposite formation and good porosity (due to the GelMA's existence in its structure). Furthermore, the hydrogel properly caused the swelling and degradation, although swelling and degradability decreased with increasing the initial concentration of GelMA. Moreover, doxorubicin release kinetics showed the non-Fickian permeation mechanism at a pH of similar to the body blood and ambient temperature. The results proposed that the PF-MNPs/GelMA composite provides a stable and controllable platform for DOX delivery. The combination of chemical interactions and physical entrapment ensures high loading efficiency, while the gradual hydrogel degradation under physiological conditions supports prolonged and predictable drug release. Although the current study provides a comprehensive characterisation and in vitro evaluation of the Pluronic PF / GelMA / iron oxide nanoparticle system, certain aspects of biocompatibility and intracellular performance were not investigated. Specifically, hemolysis assays, protein adsorption studies, immune response evaluations, as well as cellular internalisation and intracellular drug release measurements, were not performed. These represent important factors for clinical translation, and future studies will aim to systematically address these parameters to provide a more complete assessment of the nanocarrier's safety and therapeutic efficacy.

Conflict of interests

There is no conflict of interests on this research.

References

1. Jaiswal S, Dutta P, Kumar S, Chawla R. Chitosan modified by organo-functionalities as an efficient nanoplatform for anti-cancer drug delivery process. Journal of Drug Delivery Science and Technology. 62: 102407 (2021). https://doi.org/10.1016/j.jddst.2021.102407

2. Costa B, Amorim I, Gärtner F, Vale N. Understanding breast cancer: From conventional therapies to repurposed drugs. European Journal of Pharmaceutical Sciences. 151: 105401 (2020). https://doi.org/10.1016/j.ejps.2020.105401

3. Shafabakhsh R, Yousefi B, Asemi Z, Nikfar B, Mansournia MA, Hallajzadeh J. Chitosan: A compound for drug delivery system in gastric cancer-a review. Carbohydrate Polymers. 242: 116403 (2020). https://doi.org/10.1016/j.carbpol.2020.116403

4. Jain V, Kumar H, Anod HV, Chand P, Gupta NV, Dey S, et al. A review of nanotechnology-based approaches for breast cancer and triple-negative breast cancer. Journal of Controlled Release. 326: 628-47 (2020). https://doi.org/10.1016/j.jconrel.2020.07.003

5. Han HJ, Ekweremadu C, Patel N. Advanced drug delivery system with nanomaterials for personalised medicine to treat breast cancer. Journal of Drug Delivery Science and Technology. 52: 1051-60 (2019). https://doi.org/10.1016/j.jddst.2019.05.024

6. Alexandridis P, Holzwarth JF, Hatton TA. Micellization of poly (ethylene oxide)-poly (propylene oxide)-poly (ethylene oxide) triblock copolymers in aqueous solutions: thermodynamics of copolymer association. Macromolecules. 27 (9): 2414-25 (1994). https://doi.org/10.1021/ma00087a009

7. Linse P. Micellization of poly (ethylene oxide)-poly (propylene oxide) block copolymers in aqueous solution. Macromolecules. 26 (17): 4437-49 (1993). https://doi.org/10.1021/ma00069a007

8. Shen N, Hu J, Zhang L, Zhang L, Sun Y, Xie Y, et al. Doxorubicin-loaded zein in situ gel for interstitial chemotherapy of colorectal cancer. Acta Pharmaceutica Sinica B. 2(6): 610-4 (2012). https://doi.org/10.1016/j.apsb.2012.09.001

9. Shaikh IM, Tan K-B, Chaudhury A, Liu Y, Tan B-J, Tan BM, et al. Liposome co-encapsulation of synergistic combination of irinotecan and doxorubicin for the treatment of

intraperitoneally grown ovarian tumor xenograft. Journal of Controlled Release. 172 (3): 852-61 (2013). https://doi.org/10.1016/j.jconrel.2013.10.025

10. Mosafer J, Abnous K, Tafaghodi M, Mokhtarzadeh A, Ramezani M. In vitro and in vivo evaluation of anti-nucleolin-targeted magnetic PLGA nanoparticles loaded with doxorubicin as a theranostic agent for enhanced targeted cancer imaging and therapy. European Journal of Pharmaceutics and Biopharmaceutics. 113: 60-74 (2017). https://doi.org/10.1016/j.ejpb.2016.12.009

11. Mosafer J, Teymouri M, Abnous K, Tafaghodi M, Ramezani M. Study and evaluation of nucleolin-targeted delivery of magnetic PLGA-PEG nanospheres loaded with doxorubicin to C6 glioma cells compared with low nucleolin-expressing L929 cells. Materials Science and Engineering: C. 72: 123-33 (2017). https://doi.org/10.1016/j.msec.2016.11.053

12. Alyane M, Barratt G, Lahouel M. Remote loading of doxorubicin into liposomes by transmembrane pH gradient to reduce toxicity toward H9c2 cells. Saudi Pharmaceutical Journal. 24 (2): 165-75 (2016). https://doi.org/10.1016/j.jsps.2015.02.014

13. Haghiralsadat F, Amoabediny G, Sheikhha MH, Zandieh-doulabi B, Naderinezhad S, Helder MN, et al. New liposomal doxorubicin nanoformulation for osteosarcoma: Drug release kinetic study based on thermo and pH sensitivity. Chemical Biology & Drug Design. 90 (3): 368-79 (2017). https://doi.org/10.1111/cbdd.12953

14. Saravanakumar K, Hu X, Shanmugam S, Chelliah R, Sekar P, Oh D-H, et al. Enhanced cancer therapy with pH-dependent and aptamer functionalized doxorubicin loaded polymeric (poly D, L-lactic-co-glycolic acid) nanoparticles. Archives of Biochemistry and Biophysics. 671: 143-51 (2019). https://doi.org/10.1016/j.abb.2019.07.004

15. Popovici C, Popa M, Sunel V, Atanase LI, Ichim DL, Drug delivery systems based on Pluronic micelles with antimicrobial activity. Polymers. 14 (15): 3007 (2022). https://doi.org/10.3390/polym14153007.

16. Carrera Espinoza MJ, Lin K-S, Weng M-T, Kunene SC, Lin Y-S, Wu C-M. Synthesis and characterization of supermagnetic nanocomposites coated with pluronic F127 as a contrast agent for biomedical applications. Pharmaceutics. 15 (3): 740 (2023). https://doi.org/10.3390/pharmaceutics15030740

17. Attia NF, Abd El-Monaem EM, El-Aqapa HG, Elashery SEA, Abdelazeem SE, El Kady M, Khalifa SAM, Hamada, BH, El-Seedi HR, Iron oxide nanoparticles and their pharmaceutical applications. Applied Surface Science Advances. 11: 100284 (2022). https://doi.org/10.1016/j.apsadv.2022.100284.

18. Ahmadi S, Chia C-H, Zakaria S, Saeedfar K, Asim N. Synthesis of Fe_3O_4 nanocrystals using hydrothermal approach. Journal of Magnetism and Magnetic Materials. 324 (24): 4147-50 (2012). https://doi.org/10.1016/j.jmmm.2012.07.023

19. Jalili NA, Jaiswal MK, Peak CW, Cross LM, Gaharwar AK, Injectable nanoengineered stimuli-responsive hydrogels for on-demand and localized therapeutic delivery. Nanoscale. 9 (40): 15379-80 (2017). DOI: 10.1039/C7NR02327H.

20. Patel M, Bharadia P, Patel M. Formulation & evaluation of matrix type transdermal patches based on composite polymers. IJPR (1953).

21. Gibaldi M, Feldman S. Establishment of sink conditions in dissolution rate determinations. Theoretical considerations and application to nondisintegrating dosage forms. Journal of Pharmaceutical Sciences. 56 (10): 1238-42 (1967). https://doi.org/10.1002/jps.2600561005

22. Wagner JG. Interpretation of percent dissolved-time plots derived from in vitro testing of conventional tablets and capsules. Journal of Pharmaceutical Sciences. 58 (10): 1253-7 (1969). https://doi.org/10.1002/jps.2600581021

23. Higuchi T. Mechanism of sustained-action medication. Theoretical analysis of rate of release of solid drugs dispersed in solid matrices. Journal of Pharmaceutical Sciences. 52 (12): 1145-9 (1963). https://doi.org/10.1002/jps.2600521210

24. Korsmeyer RW, Gurny R, Doelker E, Buri P, Peppas NA. Mechanisms of solute release from porous hydrophilic polymers. International Journal of Pharmaceutics. 15 (1): 25-35 (1983). https://doi.org/10.1016/0378-5173(83)90064-9

25. Modaresifar K, Hadjizadeh A, Niknejad H. Design and fabrication of GelMA/chitosan nanoparticles composite hydrogel for angiogenic growth factor delivery. Artificial Cells, Nanomedicine, and Biotechnology. 46 (8): 1799-808 (2018). https://doi.org/10.1080/21691401.2017.1392970

26. Torres-Gómez N, Nava O, Argueta-Figueroa L, García-Contreras R, Baeza-Barrera A, Vilchis-Nestor AR. Shape tuning of magnetite nanoparticles obtained by hydrothermal synthesis: effect of temperature. Journal of Nanomaterials. 2019 (1): 7921273 (2019). https://doi.org/10.1155/2019/7921273

27. Gulrez SK, Al-Assaf S, Phillips GO. Hydrogels: methods of preparation, characterisation and applications. United Kingdom. Books on Demand (2011)

28. Yan Y, Cao Y, Cheng R, Shen Z, Zhao Y, Zhang Y, et al. Preparation and in vitro characterization of gelatin methacrylate for corneal tissue engineering. Tissue Engineering and Regenerative Medicine.1-14 (2022). https://doi.org/10.1007/s13770-021-00393-6

29. Choi YH, Kim S-H, Kim I-S, Kim K, Kwon SK, Hwang NS. Gelatin-based micro-hydrogel carrying genetically engineered human endothelial cells for neovascularization. Acta Biomaterialia. 95: 285-96 (2019). https://doi.org/10.1016/j.actbio.2019.01.057

30. Li Y, Liu J, Dong H, Liu G, Hu H. Engineering of a Pluronic F127 functionalized magnetite/graphene nanohybrid for chemophototherapy. Nanotechnology. 25 (6) 065602 (2014). doi: 10.1088/0957-4484/25/6/065602.

View Article Online
DOI: 10.1039/D5NA00776C

31. Yang X, Zhang X, Liu Z, Ma Y, Huang Y, Chen Y. High-efficiency loading and controlled release of doxorubicin hydrochloride on graphene oxide. Journal of Physical Chemistry C. 112 (45) 17554–58 (2008). https://doi.org/10.1021/jp806751k.

32. Heredia NS, Vizuete K, Flores-Calero M, Pazmiño V K, Pilaquinga F, Kumar B, Debut A. Comparative statistical analysis of the release kinetics of hydrophilic and lipophilic compounds from hydrogel systems. Pharmaceutical Research. 17(3): e0264825 (2022). doi: 10.1371/journal.pone.0264825.

33. Costa P, Lobo JMS. Modeling and comparison of dissolution profiles. European Journal of Pharmaceutical Sciences. 13 (2): 123-33 (2001). https://doi.org/10.1016/S0928-0987(01)00095-1

View Article Online
DOI: 10.1039/D5NA00776C

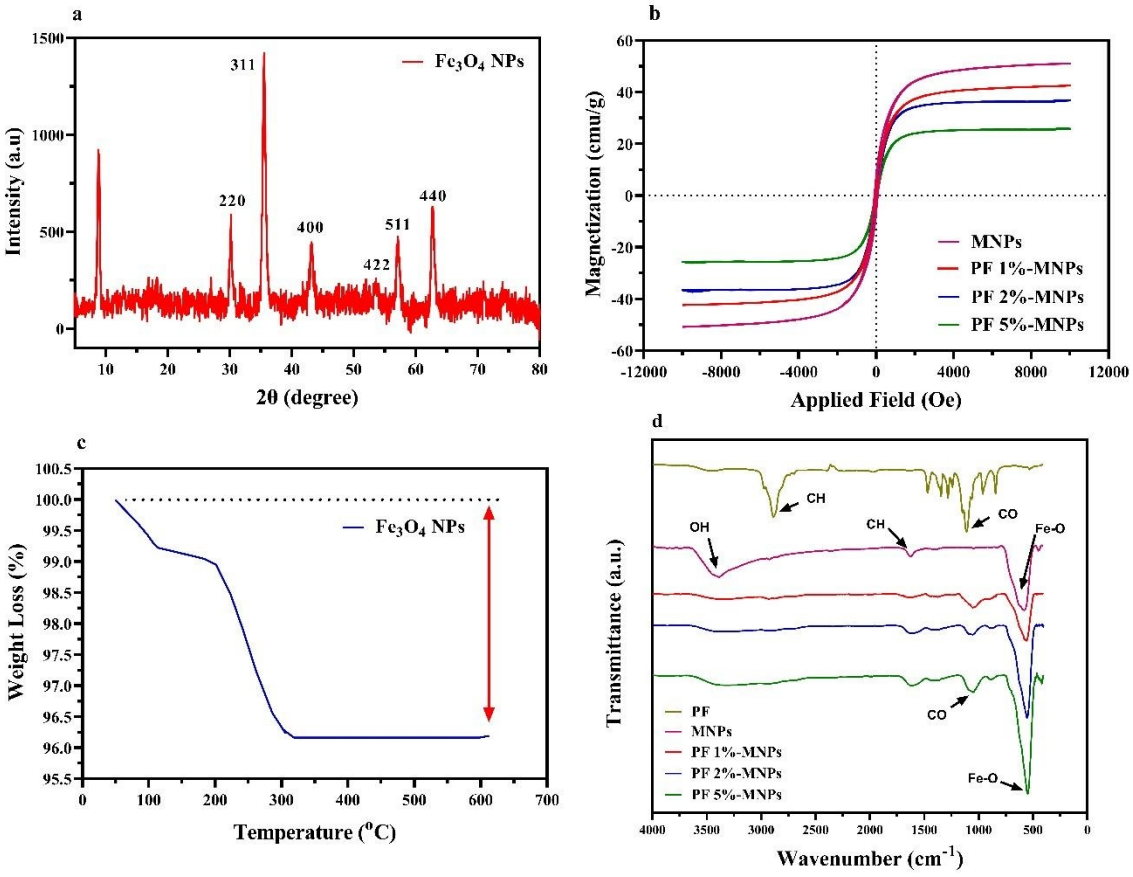

Fig 1. a) XRD of iron oxide nanoparticles, b) Magnetic curve of MNPs, c) TGA analysis curve of MNPs, and d) FTIR spectra of PF, MNPs, and three various concentrations of PF-MNPs

View Article Online
DOI: 10.1039/D5NA00776C

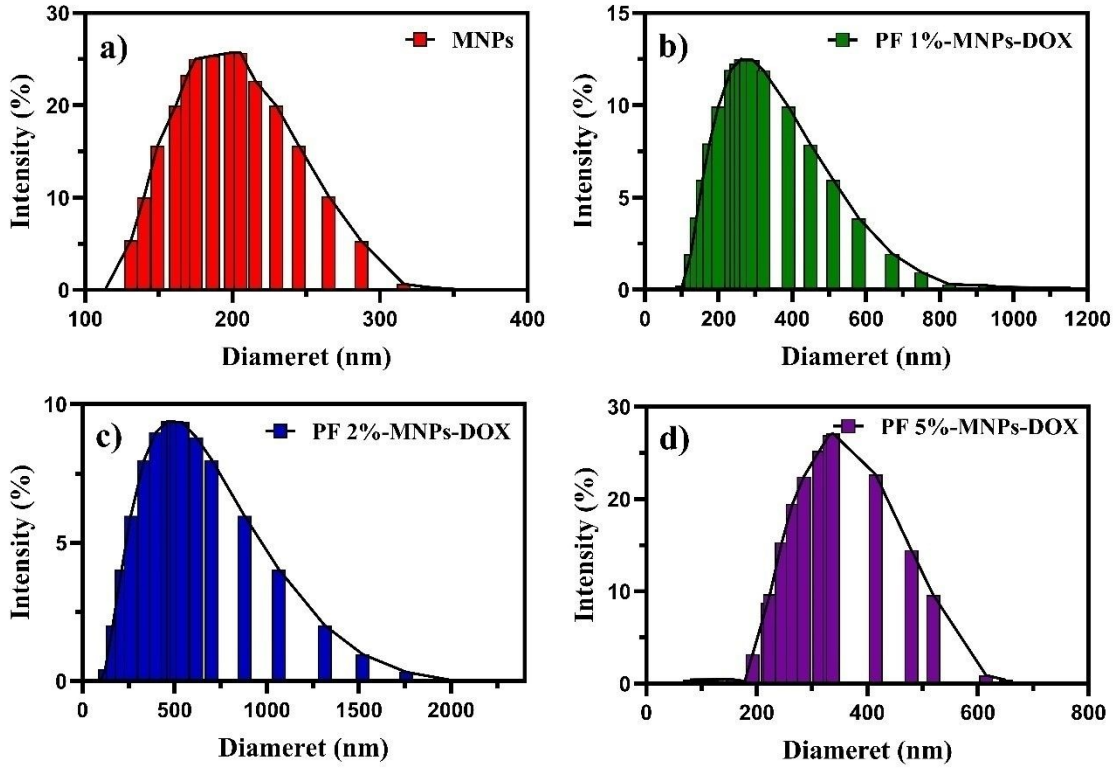

Fig. 2. Dynamic light scattering particle size distribution of a) pure MNPs, b) PF 1%-MNPs-DOX, c) PF 2%-MNPs-DOX, and d) PF 5%-MNPs-DOX

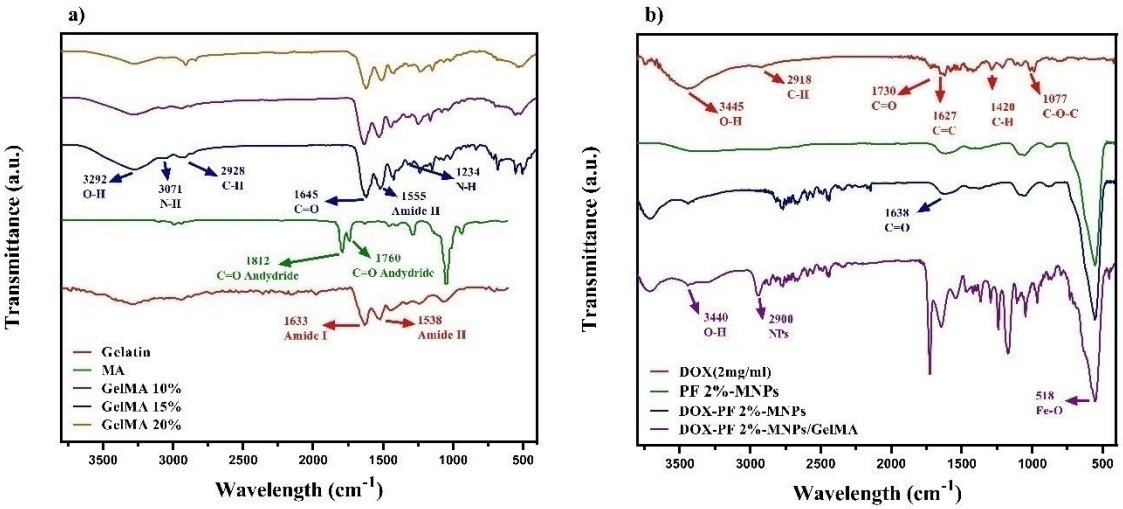

Fig. 3. FTIR spectra of a) Gelatin, GelMA (with three different percentages), and b) DOX, PF 2%-MNPs, DOX-loaded nanoparticles, and DOX-PF 2% MNPs blended on GelMA (15%)

View Article Online
DOI: 10.1039/D5NA00776C

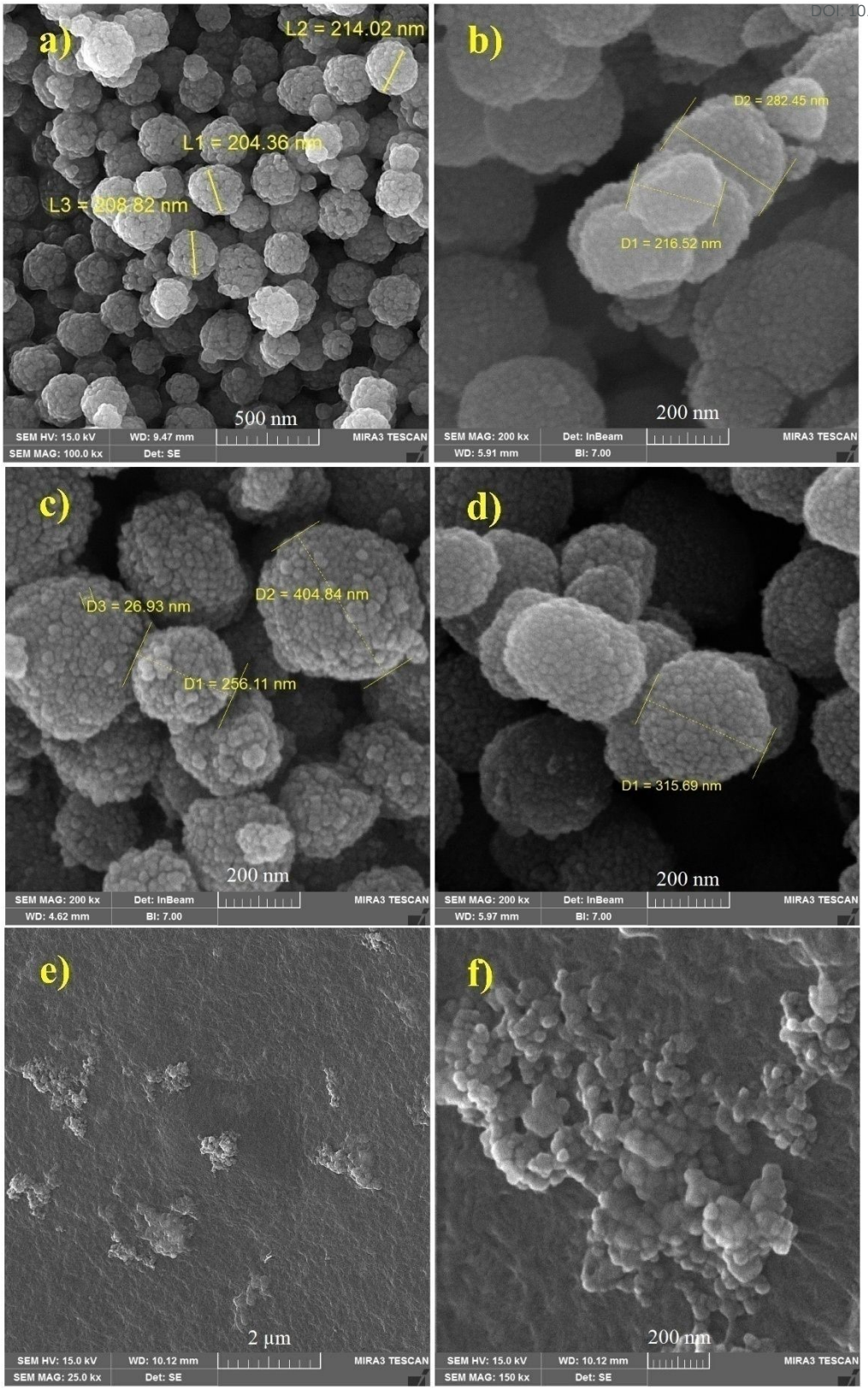

Fig. 4. FESEM images of a) pure MNPs, b) PF 1% with MNPs, c) PF 2% with MNPs, d) PF 5% with MNPs, and e & f) DOX-loaded PF 2%-MNPs blended on GelMA (15%)

View Article Online
DOI: 10.1039/D5NA00776C

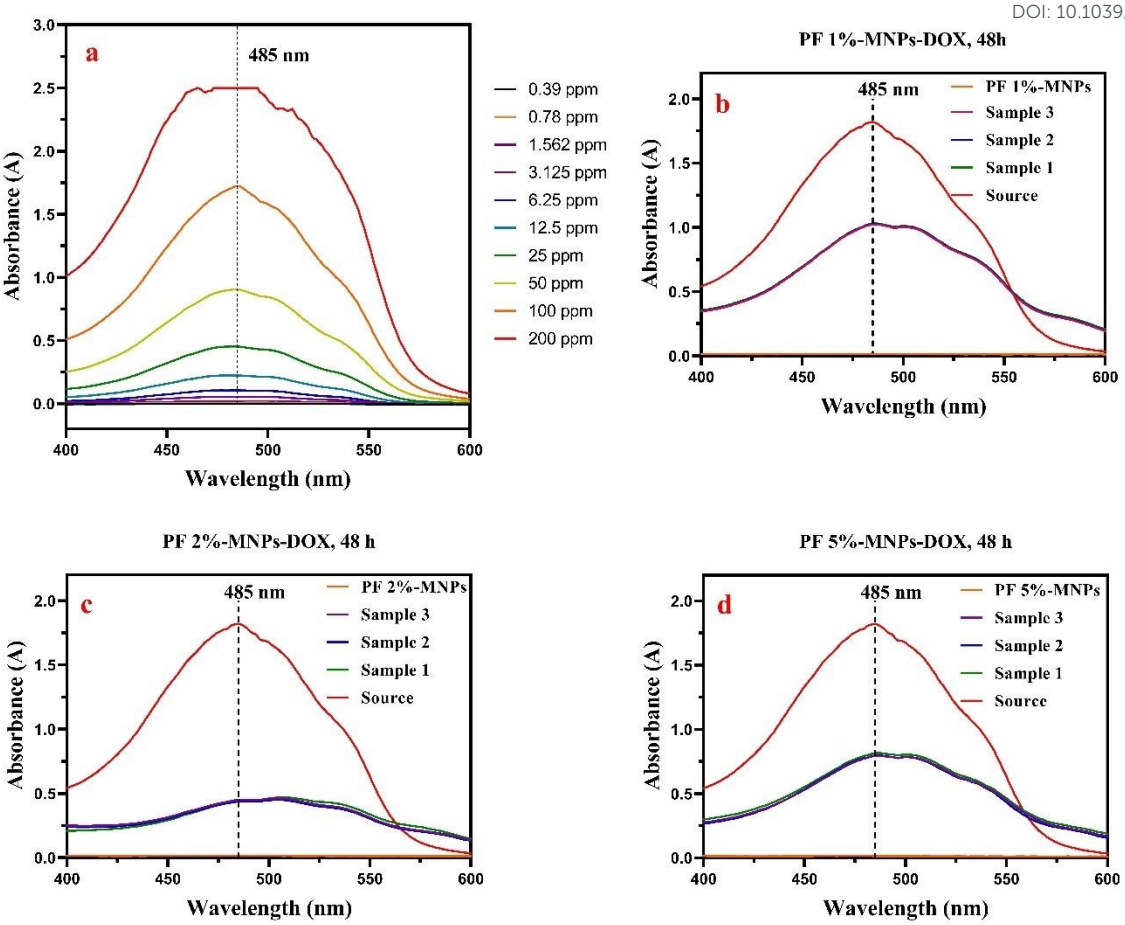

Fig. 5. UV-Vis spectra for a) free DOX, b) PF 1%-MNPs-DOX, c) PF 2%-MNPs-DOX, and d) PF 5%-MNPs-DOX

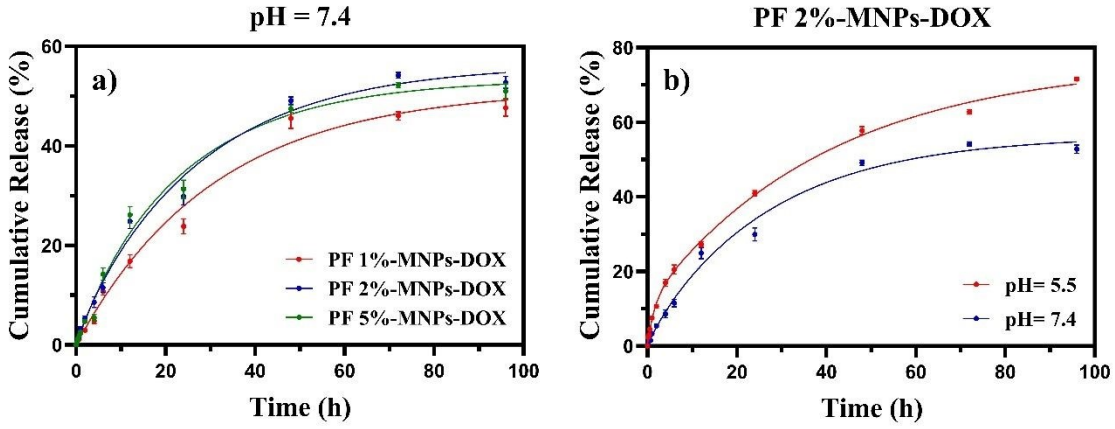

Fig. 6. Release pattern of a) DOX from DOX-loaded MNPs-PF with three different percentages of PF coated on MNPs at pH of 7.4, and b) PF 2%-MNPs-DOX at two different pH levels (7.4 and 5.5)

View Article Online
DOI: 10.1039/D5NA00776C

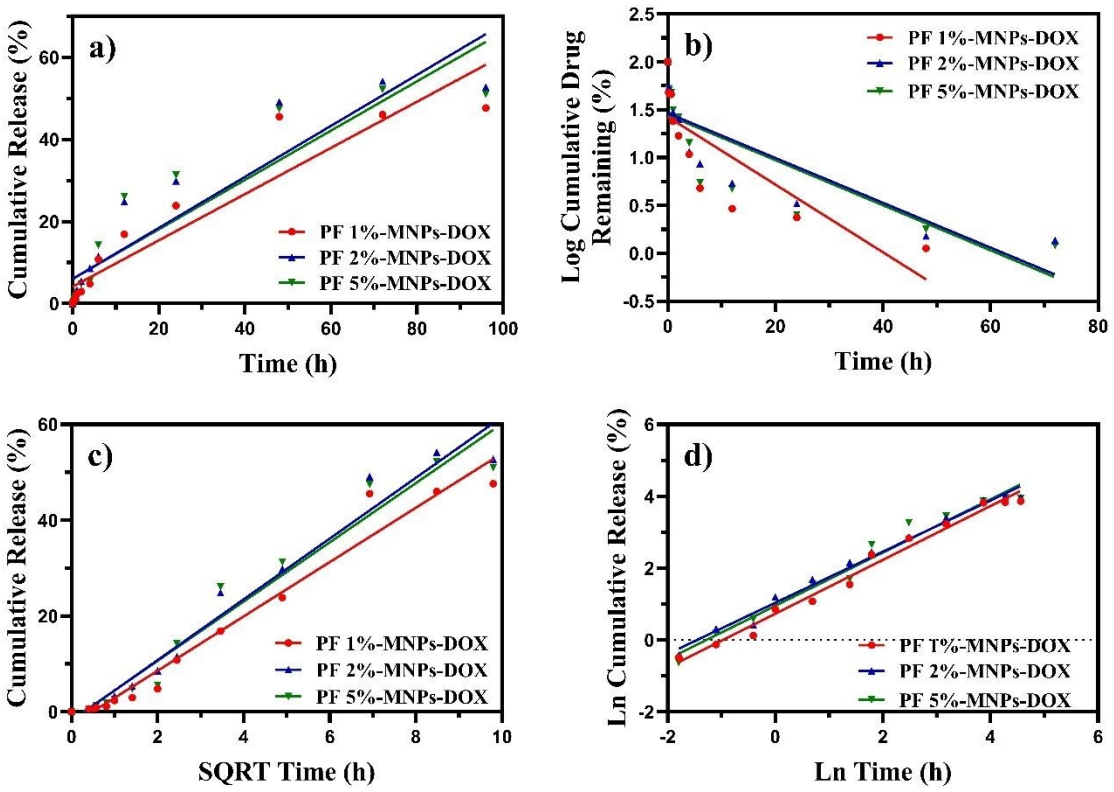

Fig. 7. Various models for DOX release at pH of 7.4 for 2% Pluronic nanocomposite a) zero-order b) first-order c) Higuchi d) Korsmeier-Peppas models

View Article Online
DOI: 10.1039/D5NA00776C

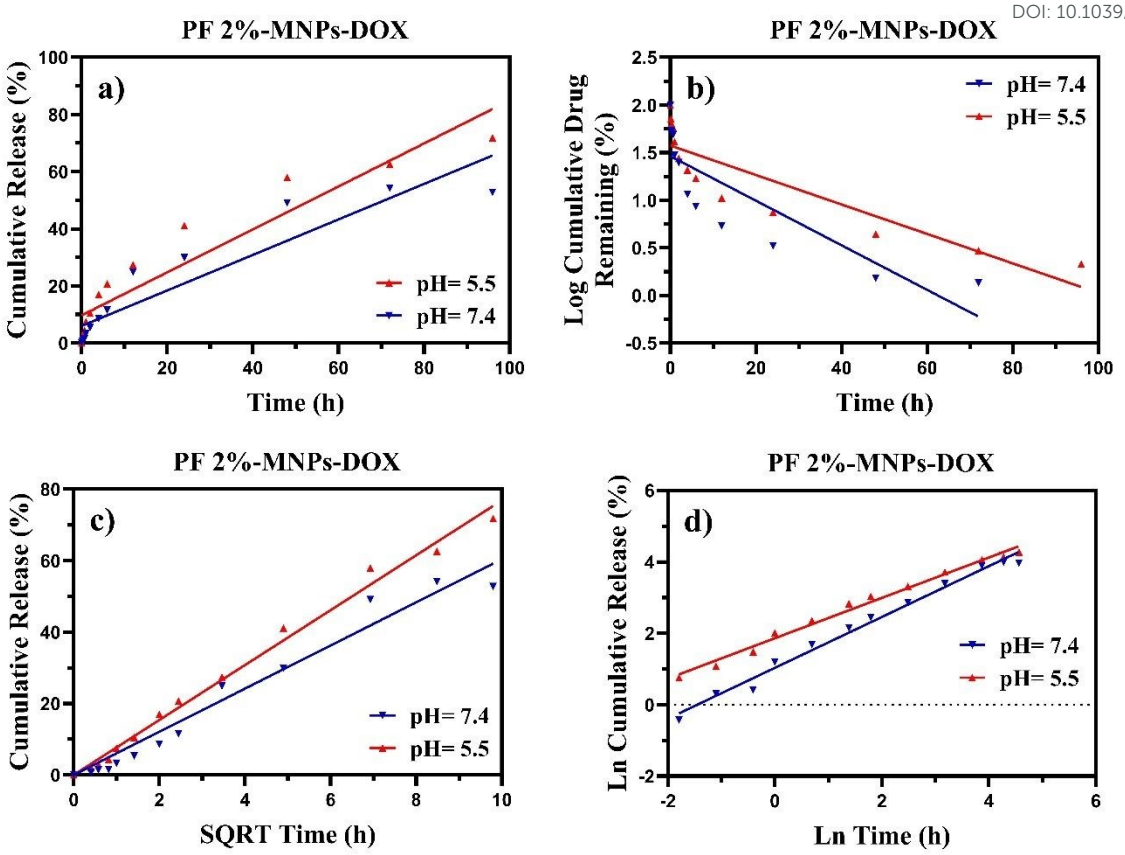

Fig. 8. In vitro release profile of PF 2%-MNPs-DOX under different pH levels (7.4 and 5.5) at 37 °C, a) zero-order, b) first-order, c) Higuchi, and d) Korsmeier-Peppas models

View Article Online
DOI: 10.1039/D5NA00776C

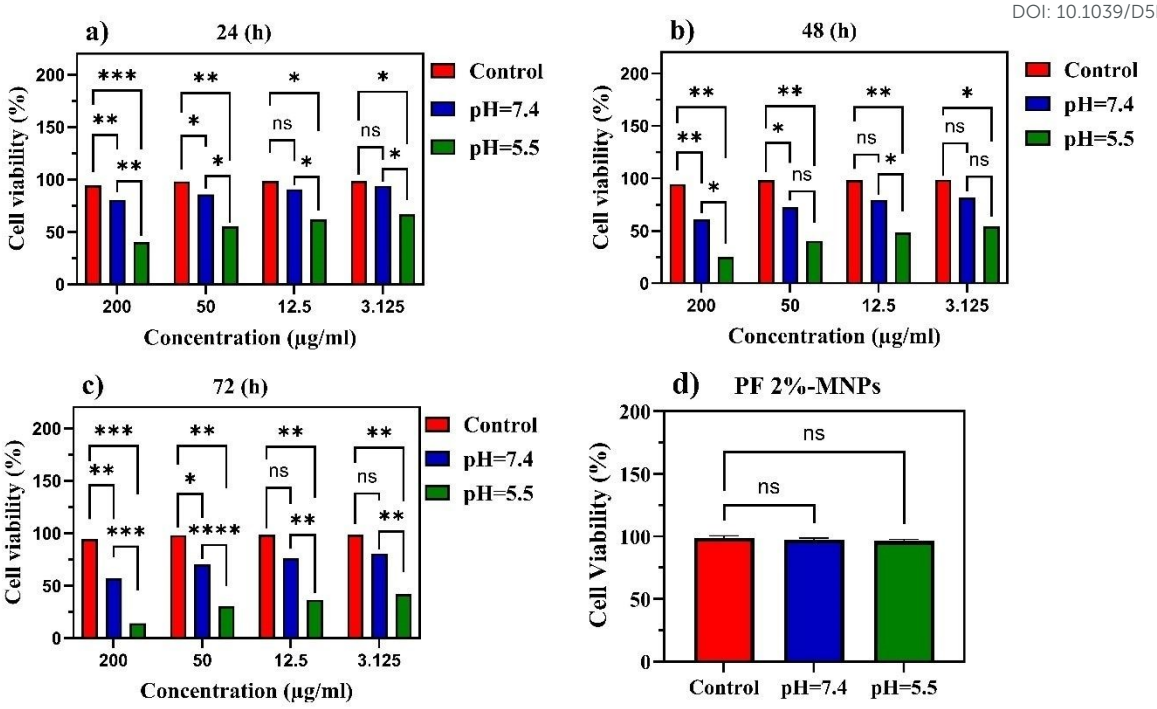

Fig. 9. Cell viability of PF 2%-MNPs and DMED media over the MCF-7 cell line at different pHs, a) 24, b) 48 and c) 72 h for four different concentrations of DOX, and d) carrier without DOX
Notes: *denotes P < 0.05, **denotes P < 0.01, ***denotes P < 0.001, and ****denotes P <0.0001

Table 1. Particle size and zeta potential of samples with different PF127 contents at various pHs (1 atm and 37 °C).

Sample Code	pH	Zeta (mV)	SD (mV)	Particle Size (nm)	PDI
MNPs	7.4	-31.5	6.84	189.3	0.217
PF 1%-MNPs-DOX	7.4	-28.3	7.61	264.8	0.192
PF 2%-MNPs-DOX	7.4	-15.1	10.4	445.3	0.440
PF 5%-MNPs-DOX	7.4	-12.3	65.8	338.9	0.176
PF 1%-MNPs-DOX	5.5	-14.54	8.58	243.6	0.205
PF 2%-MNPs-DOX	5.5	-10.58	15.6	437.5	0.305
PF 5%-MNPs-DOX	5.5	13.2	7.76	319.8	0.198

Table 2. Swelling percentage of GelMA hydrogels at different concentrations measured at 24 h (Mean ± SD, n = 3)

GelMA (%)	W_d (mg)	W_t (mg)	$W_{t=10}$ (mg)	SC_t (%)	$SC_{t=10}$ (%)
10	23.39	101.28	85.90	213.2 ± 14.3	165.1 ± 16.6
15	44.70	150.28	118.50	237.0 ± 19.0	165.0 ± 9.2
20	88.60	282.52	234.10	218.9 ± 5.90	164.9 ± 3.6

View Article Online
DOI: 10.1039/D5NA00776C

Table 3. Degradation of GelMA hydrogels at different concentrations measured over 90 days [Mean ± SD, n = 3 (Fig. S2)]

GelMA (%)	W_d (mg)	W_t (mg)	Percentage of degradation (%)
10	40.92	14.88	63.5 ± 3.3
15	50.45	16.25	67.8 ± 2.5
20	76.19	45.97	39.6 ± 1.4

Table 4. Drug entrapment efficiency (%) of different nanoparticle samples (Mean ± SD, n = 3)

PF -MNPs	EE%	DLE%
1%	43.61±0.251	1.52±0.009
2%	74.73±0.549	2.60±0.019
5%	55.87±0.610	1.94±0.022

Table 5. Correlation coefficients of the fit of each model for nanocarriers at pH=7.4 and pH=5.5

Composite					
	Zero order	First order	Higuchi	Korsmeyer-Peppas	
pH= 7.4	R^2	R^2	R^2	R^2	n
PF 1%-MNPs-DOX	0.8901	0.6761	0.9675	0.9827	0.7497
PF 2%-MNPs-DOX	0.8698	0.7206	0.9710	0.9860	0.7120
PF 5%-MNPs-DOX	0.8481	0.6885	0.9620	0.9745	0.7418
pH=5.5					
PF 2%-MNPs-DOX	0.8934	0.7812	0.9912	0.9876	0.5649

View Article Online
DOI: 10.1039/D5NA00776C

Data availability

Data underlying the results presented in this paper are not publicly available at this time but may be obtained from the authors upon reasonable request.